Graphene-Veiled Gold Substrate for Surface-Enhanced Raman Spectroscopy

*Weigao Xu, Jiaqi Xiao, Yanfeng Chen, Yabin Chen, Xi Ling, and Jin Zhang**

Surface-enhanced Raman spectroscopy (SERS)[1–3] can boost the pristine Raman signal by 10^8 times or more, which has exhibited amazing potential for ultrasensitive analytical applications. However, the inherent complexity of a SERS system makes this a "double-edged sword". The high sensitivity of SERS (even capable for detection of a single molecule[4,5]) is dimmed by its poor reproducibility (which makes it difficult for peak-to-peak assignment of each vibrational mode). By the virtue of wide achievements on miscellaneous substrate preparation methods, both the understanding of the enhancement mechanism of SERS and the pursuit of more desirable SERS signals have taken impressive steps forward. Nevertheless, there remains more to be further investigated.[6,7] To improve signal cleanliness against substrate-induced fluctuations and to investigate the detailed SERS activity–morphology relationship are two important aspects, both of which are critical for "out of the laboratory" applications of SERS. In the present study, we exploited graphene to fabricate a veiled, rough, gold substrate for SERS. The graphene-veiled gold substrate inherits the concept of metal–molecule isolation,[8,9] providing a passivated surface for SERS which exhibits good signal reproducibility. By tuning the morphology of the gold–graphene combined structure, the detailed electromagnetic enhancement activity–morphology relationship is investigated.

Actually, among the various concerns about the performance of a SERS substrate, the issue of metal–molecule contact induced signal variations has become a subject with rising importance.[8,9] The main unfavourable disturbances include chemical adsorption-induced vibrations, charge transfer between the metal and molecules, photo-induced damage and metal-catalyzed side reactions, etc.[6] Using a thin and pinhole-free layer of SiO_2 or Al_2O_3 as an inert shell,[8] Tian's group demonstrated a series of measurements which are challenging with a normal metal substrate. Fabrication of SERS substrates with a passivated surface at a lowest loss of electromagnetic enhancement activity is the key to shell-isolated SERS. Till now, both atomic layer deposition (ALD)[10] and wet chemistry approach[8] appeared to be possible methods. The main challenge is to get a pinhole-free coating layer with a very small thickness (to prevent substrates from apparent loss of the electromagnetic enhancement activity). The unique structure (the atomic thickness and seamless structure) of graphene makes it a natural candidate material for shell-isolated SERS. Actually, recently we succeeded in collecting cleaner and more reproducible SERS signals on a flat graphene surface.[9]

In addition, exploring the structure–(SERS performance) relationship is a long-term pursuit, and great efforts towards this goal have been reviewed recently.[11] Theoretically, the electromagnetic enhancement problems can be addressed by solving the Maxwell's equations, but usually both the uncontrollable molecular distribution and various inevitable chemical interactions complicate the evaluation of the electromagnetic contribution. Thus, the study of the distance-dependent electromagnetic enhancement is usually hindered. Till now, only a few studies have been carried out,[12,13] and apparently our current knowledge is too limited.

Graphene, a 2D atomic crystal with densely packed carbon atoms in a honeycomb crystal lattice,[14] is well-known for its unique electrical performance and the amazing applications in nanoscale electronics.[15] As well as the wide interest in its electric properties, graphene is also a rising star in Raman spectroscopy.[16] Representative studies include both the intriguing Raman modes of graphene itself[17,18] and Raman behaviours of graphene derivatives/graphene-based composites.[19–21] Recently, graphene-involved SERS studies have also received much attention. First, graphene itself was found to be active for Raman enhancement of adsorbed molecules, referred to as the graphene-enhanced Raman scattering (GERS) effect.[22,23] In our earlier work, detailed studies on GERS including the first-layer effect,[24] molecular orientation effect,[25] and the electric field effect (Fermi level modulation)[26,27] indicate that the GERS enhancement is based on a chemical enhancement mechanism. On the other hand, graphene–metal nanoparticle composites are also explored in SERS, in which graphene is suggested to serve as: a fluorescence quencher,[28] an additional chemical enhancer,[23] a molecule enricher,[29–31] and a building block of an atomically flat SERS substrate.[9]

In this work, we provide a "two-step" approach to prepare an active, graphene-veiled gold substrate. As a building block of shell-isolated SERS substrate in a new form, graphene serves as an atomically thin, seamless, and chemically inert net with dual functions: 1) graphene prevents metal–molecule chemical interactions and thus is anticipated to simplify the electromagnetic enhancement problem; 2) graphene keeps molecules at a

W. G. Xu, J. Q. Xiao, Dr. Y. F. Chen, Y. B. Chen, Dr. X. Ling, Prof. J. Zhang
Center for Nanochemistry
Beijing National Laboratory for Molecular Sciences
Key Laboratory for the Physics and Chemistry of Nanodevices
State Key Laboratory for Structural Chemistry of Unstable and Stable Species
College of Chemistry and Molecular Engineering
Peking University
Beijing 100871, China
E-mail: jinzhang@pku.edu.cn

DOI: 10.1002/adma.201204355

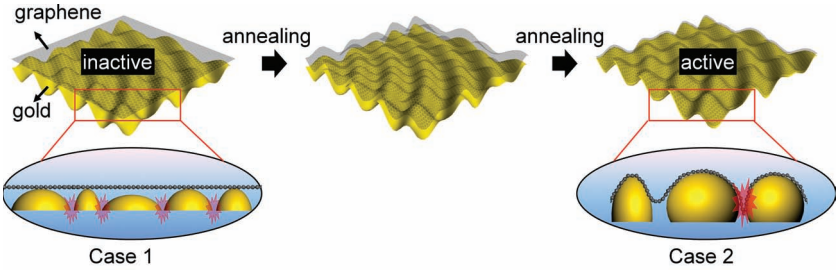

Scheme 1. Schematic illustration of graphene-veiled SERS substrates with graphene spread over the curved side of gold nanoislands in two cases, which exhibit distinguished electromagnetic enhancement activity. Here an 8-nm film of gold nanoislands was used as the electromagnetic enhancer. Case 1 (SERS inactive) and case 2 (SERS active) are the cases before and after an activation process of thermal annealing, respectively.

certain position and thus enables the investigation of position-sensitive electromagnetic enhancement activity.

Gold film prepared by vacuum thermal evaporation and graphene prepared from mechanically exfoliated Kish graphite[14] were used in our experiments. According to the well-known surface plasmon resonance (SPR) effect, gold nanoislands focus the incident laser, creating electromagnetic hot spots at their nanogaps. The resulting huge enhancement of the Raman scattering signals of molecules in close vicinity is called the electromagnetic enhancement, which is considered to be the dominant contribution of the SERS enhancement. Since localized hot spot attenuates, in an exponential way (with distance away from the central strongest point),[32] the SERS activity of a substrate is highly position sensitive. According to our earlier observations, an 8-nm gold film can provide nanoislands with very small gaps of the size of 2–3 nm,[9] which guarantees considerable SERS activity. As illustrated in **Scheme 1**, by transferring mechanically exfoliated graphene onto an island-like 8-nm gold film (case 1), graphene-veiled gold substrate can be fabricated directly, with the curved side of gold nanoislands adhered to graphene. Since for a graphene-veiled gold substrate the SERS enhancement of gold is mediated by the graphene layer, thus we will call the enhanced signals from a graphene-veiled gold substrate as "G-SERS" (graphene-mediated SERS) signals in the following.

A graphene veil can totally change the electromagnetic enhancement behaviour of an island-like gold film. As will be described below, in this work the SERS activity of case 1 was examined, which exhibited an electromagnetic enhancement inactive behaviour. Then we implemented a thermal annealing procedure to "activate" the inactive substrate. Detailed experimental route is schematically shown in Figure S1 (of the Supporting Information (SI)). The as-prepared inactive substrate was annealed at 400 °C for 2 h (in a protective atmosphere of Ar and H_2) to make better contact between graphene and the gold film. As illustrated in Scheme 1 (case 2), after annealing, gold nanoislands aggregated into larger nanoparticles, and at the same time the flat graphene layer wrinkled, therefore, improving the contact state with the underlying gold nanoislands. Wrinkled graphene is supposed to get closer to the electromagnetic "hot" spot and thus allows a large increase on the final SERS activity.

During the practical process of sample preparation, two aspects should be noted. First, the visibility of the exfoliated graphene on the gold film should be considered. A silicon substrate with an oxide layer about 300 nm thick is suitable for the visibility of single layer graphene,[33,34] but on a gold-film-coated SiO_2/Si substrate, the colour contrast of graphene is modified. As shown in **Figure 1**a, for the case of an 8-nm gold layer before annealing, single layer graphene (1LG) is invisible and bilayer graphene (2LG) is only hardly distinguished because of the low colour contrast. After an annealing process, both the optical colour of the substrate and of the graphene are altered, and even single layer graphene become clearly visible (Figure 1b), which will benefit the implementation of locating graphene-veiled regions on the substrate of thin-layer graphene-coated gold nanoislands. Second, the morphology of the gold film has been changed. Figure 1c and d show the corresponding SEM images of a piece of bilayer graphene on the substrate before and after annealing. Consistent with earlier investigations on the adsorption properties for the gold-on-graphene system,[35,36] it is here seen that, after thermal annealing, gold nanoislands melted and aggregated into bigger nanoparticles. Their sizes are from tens to hundreds of nanometres. Although the optical image shows high colour contrast between the graphene-veiled and bare gold regions, the SEM morphology of gold nanoislands

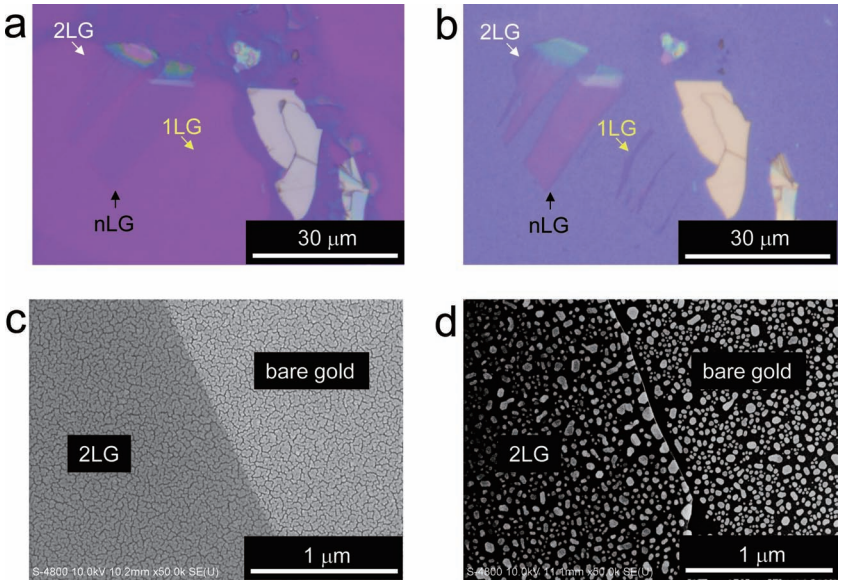

Figure 1. Optical and SEM images of exfoliated graphene on Au/SiO_2/Si substrate before and after annealing. a,b) Optical images of graphene on an 8-nm gold film a) before, and b) after annealing. Single layer (1L-), bilayer (2L-), and few-layer (nL-) graphene pieces are marked with arrows. c,d) SEM images of a 2LG on an 8-nm gold film c) before, and d) after annealing.

ADVANCED MATERIALS
www.advmat.de

www.MaterialsViews.com

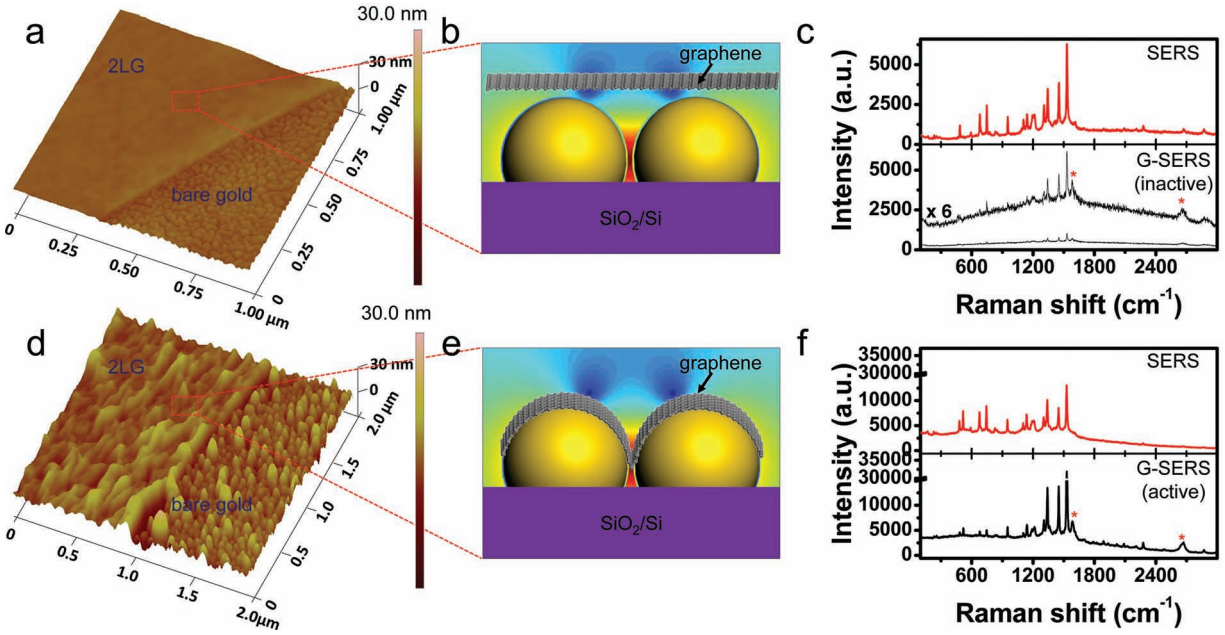

Figure 2. Morphology-dependent SERS performance of normal SERS and G-SERS regions. a,d) AFM images of a 2LG-covered 8-nm gold film a) before, and d) after annealing, showing both the bare gold regions and the graphene-covered regions. b,e) Schematic illustration of the contact state between the graphene and the gold nanostructures that correspond to the enlarged regions. c,f) SERS performance of normal SERS (top) and G-SERS regions (bottom) c) before, and f) after annealing, respectively. "*" marks the G and G′ band of the bilayer graphene (2LG).

in the regions with and without a bilayer graphene cover layer is similar (Figure 1d). This is possibly due to the fluorescence quenching effect of graphene, as will be discussed later in the following.

Atomic force microscopy (AFM) was also used to characterize the morphology of the graphene-veiled gold samples. **Figure 2**a and d are AFM images of a bilayer graphene piece on an 8-nm gold film before and after annealing. For comparison, two distinguished regions (i.e., the bare gold region and graphene-veiled region) are shown together. As also was observed from the SEM images, the morphology variation (shape and size) of gold nanoislands during the annealing process is observed. Simultaneously, AFM images also show a clear morphology change of graphene. As shown in Figure 2a, the surface of pristine graphene was flat, after annealing it changed to a wrinkled morphology with much larger surface roughness. It is anticipated that, thermal annealing process allows graphene to get in better contact with the underlying gold nanostructures. Then, the electromagnetic "hot" spots get closer to the graphene surface and make the final combined structure electromagnetic enhancement active, to enhance the Raman signals of adsorbates.

Furthermore, we checked the SERS performance of the as-prepared substrate. Regions with and without a bilayer graphene veil are tested, corresponding to the normal SERS region (reference measurements) and the G-SERS region. Copper phthalocyanine (CuPc) was deposited by vacuum thermal evaporation (1 Å, which is less than a monolayer. This method can bring down the adsorption-induced variations on the amounts of molecules) and its pristine Raman spectra were measured (shown in Figure S2b of the SI). The SERS and G-SERS spectra of CuPc are shown in Figure 2c and f. For samples before annealing, the SERS and G-SERS regions exhibit distinguished SERS activity, and agreed well with our predictions. As shown in Figure 2c, for SERS regions, signals with acceptable intensity can be obtained. While the CuPc signal at G-SERS regions is much weaker than that of the SERS regions without graphene, with a pretty bad signal-to-noise ratio (a magnified view of ×6 is also shown for comparison). This result suggests that, in a pristine graphene-veiled substrate before activation, the gold film is not an effective electromagnetic enhancer of the Raman signal of CuPc on graphene. As Mie theory and three-dimensional finite difference time domain (3D-FDTD) simulation results show that the thin graphene layer will not cause the enhanced electromagnetic field between gold nanostructures to obviously decay,[9] here we anticipate that the current poor activity is due to the SERS-active hot spots being "buried" under a graphene veil at a distance away. This is also consistent with our AFM observations. It should be noted that, although it was claimed that a conductive graphene layer suppresses the surface electric field,[37] it is not considered to be the reason of the weak SERS activity for an inactive G-SERS substrate, because it can be further thermally activated (without changing the conductivity of graphene, as will be described below).

On the other hand, as shown in Figure 2f, after the activation process by thermal annealing, the SERS performance of both regions is modified. The first intriguing effect is that the Raman scattering signal of the G-SERS region is hugely enhanced, which indicates an effective activation of the pristine, inactive G-SERS substrate. Meanwhile, for SERS regions the band features of CuPc are also modified. As compared with SERS spectra of pristine gold film, thermal annealing results

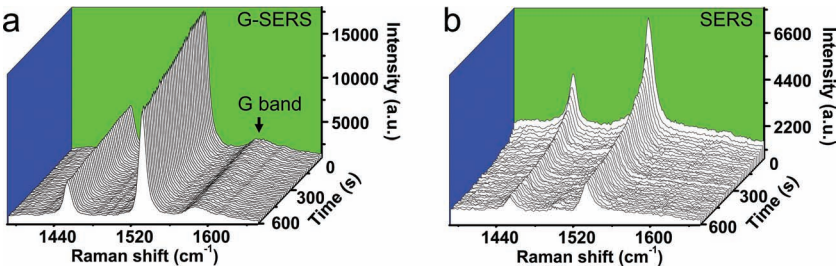

Figure 3. Stability of the enhanced Raman signal of CuPc by a) G-SERS, and b) normal SERS, after thermal annealing activation. Laser power is 0.2 mW, each panel has 44 spectra in total, and each spectrum has an acquisition time of 5 s. The peak at 1586 cm^{-1} in (a) is the G band of graphene.

in an enhancement in the lower frequency region, while in the higher frequency region of 1800–3000 cm^{-1}, most of the spectral features of the overtones of CuPc are almost unrecognizable. This result is apparently different from that of the SERS spectra using a gold film without annealing, in which the spectral information at 1800–3000 cm^{-1} is clear. The pristine- (on a SiO_2/Si substrate) and GERS-spectrum (on a 2LG/SiO_2/Si substrate) of CuPc are also shown in Figure S2b of the SI. We find an interesting phenomenon that, G-SERS tends to provide a greatly enhanced GERS signal, while keeping the pristine band features of GERS. Actually in our previous results, the graphene layer was also proven to reduce the SERS signal variations of Rhodamine 6G between gold and silver substrates.[9] This indicates that, G-SERS substrate tends to provide a surface with more well-defined molecule–substrate interactions, resulting in enhanced Raman signals with highly consistent band features, regardless of the material and morphology of the metal nanostructures which would change the SERS results.

Furthermore, as a seamless and chemically inert passivation layer, an additional effect of graphene is stabilization. As shown in **Figure 3**, time-dependent experiments were also carried out to compare the stability of the SERS and G-SERS spectra. During a 600 s measurement, the signal of CuPc in the normal SERS region decreased quickly in intensity while in the G-SERS region it was much more stable. Besides a considerable surface passivation effect,[9,38] this stabilization effect should also be related to the graphene–CuPc interactions. As for CuPc molecules adsorbed on a flat graphene surface, the signal stabilization effect is observed[9] and the formation of a graphene/CuPc complex (possibly through π–π interactions) is shown by the UV-visible absorption spectra in our recent results.[25] Here we see that, despite the high surface roughness of wrinkled graphene in an activated G-SERS substrate, this stabilization effect remains prominent. It should be noted that, the stabilization effect for different molecules is case-dependent, but it could be general for aromatic molecules, especially for those which have a strong interaction with graphene.

In-situ Raman measurements were carried out using a Linkam CCR1000 heating stage to investigate the kinetic activation process of graphene-veiled substrates. A piece of bilayer graphene on an 8-nm gold film (Figure S3 of the SI) was heated from 25 to 400 °C in an Ar+H_2 atmosphere, in 25 °C steps and held for 5 min after each step for recording Raman measurements. It should be noted that, graphene itself is a perfect Raman probe for the SERS activity of the substrate. As shown in **Figure 4**, at first the intensity of the G and G′ bands of graphene increases with the rising temperature, it reaches a maximum at 175 °C (yet this does not indicate the optimum SERS enhancement since the temperature-induced decrease of Stokes Raman signals should be taken into consideration) and remains at a stable intensity level (with only a small decrease) during the continued heating process (Figure S4 of the SI). Further increased heating temperature (above 550 °C, for our observation) will cause damage to graphene. During the thermal annealing process, the flat graphene piece wrinkles and so its contact with the underlying gold film is gradually improved. The closer electromagnetic "hot" spots to the graphene surface will cause a larger SERS enhancement of the graphene signals. A certain quantity of close-packed gold nanoislands are responsible for the dominant enhancement, yet there is certain amount of the Raman enhancement that should be attributed to the isolated gold nanoislands. Additionally, by looking at the fluorescence background of the obtained Raman spectra, we find the photoluminescence property of the graphene-on-gold system (as well as bare gold) is highly morphology dependent (Figure S4 of the SI). For the bare 8-nm gold film region, there is a broad photoluminescence background centered at 1260 cm^{-1} (687.6 nm). During the thermal annealing process from room temperature

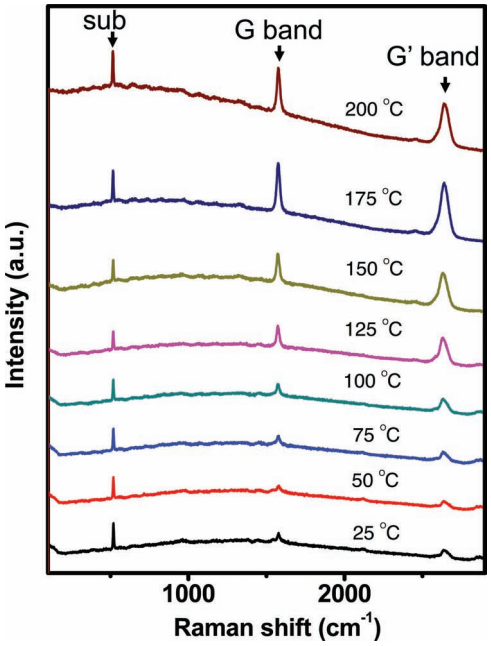

Figure 4. In-situ monitoring of the activation process of a 2LG-veiled gold substrate heated form 25 to 200 °C in a protective atmosphere. Spectra of the continued temperature range (225 to 400 °C) and spectra of bare gold region (normal SERS) are shown in Figure S4 of the SI. Peaks of the Si substrate (sub), the G and G′ band of graphene are marked with arrows, respectively.

to 200 °C, the relatively weak photoluminescence background becomes stronger, accompanied by a gradual blue shift to 584 cm^{-1} (657.1 nm) at 200 °C. Further increase of the temperature causes decreasing photoluminescence intensity (while there are no clear shifts). Compared with the bare gold region, the graphene-veiled region keeps a low photoluminescence background, which is also a rigorous proof for the graphene–gold interactions. Thus, thermal annealing increases the difference between the photoluminescence properties of bare gold and graphene-veiled gold region, it may also be the reason for an increased colour contrast for the two regions as observed from the optical images. It could thus be confirmed that annealing will improve the graphene–gold contact, thus resulting in the enhancement of the Raman signal of graphene.

In summary, we demonstrated a two-step procedure for the fabrication of an active, graphene-veiled substrate. Unlike most other SERS substrates, where molecules are directly adsorbed on the active metal surface, this new kind of substrate provides a passivated surface for SERS. The graphene veil enables SERS analysis with more well-defined molecular interactions and thus results in enhanced Raman signals with improved reproducibility. This work provides a unique strategy towards the design of surface-passivated SERS substrates with the lowest loss of SERS activity. We anticipate our results will benefit the design and fabrication of a more desirable SERS substrate. In addition, by virtue of the unique structure and characteristic Raman signal of graphene, this work demonstrates an amazing platform for the investigation of the morphology–(SERS performance) relationship, and is expected to shed light on the finer details of SERS enhancement.

Experimental Section

Construction of graphene-on-gold structure: gold wire (purity>99.9%, 0.25 mm) was used as the source for vacuum thermal evaporation (UNIVEX-300, oerlikon leybold vacuum). 8-nm gold films were deposited on SiO_2(300 nm)/Si substrates at a rate of about 1 Å/s, and at a pressure of about 10^{-3} Pa. Before the transfer of graphene, the as-prepared gold film was then treated by O_2-plasma for both surface cleaning and a better affinity with graphene. Mechanically exfoliated graphene was then transferred from Kish graphite (Covalent Materials Corp.) using a scotch tape.[14]

Thermal annealing activation and characterization: For activation of the pristine graphene-veiled gold substrate, sample was heated to 400 °C for 2 h in an Ar+H_2 atmosphere. Optical microscopy (OM, Olympus BX51), scanning electron microscopy (SEM, Hitachi S4800), atomic force microscopy (AFM, Nanoscope III(a)) and Raman spectroscopy (Horiba HR800, with a 632.8 nm line from a He-Ne laser and a full laser power of about 2.5 mW under the microscopy, the size of the laser spot is about 1 μm) was used to characterize the morphology and SERS performance of the normal SERS and G-SERS regions. Copper phthalocyanine (CuPc) from Alfa-Aesar was used as Raman probe directly as received, chemical structure is shown in Figure S2a of the SI. All spectra in comparison were obtained under the same conditions.

In-situ Raman measurements: Linkam CCR1000 heating stage (accompanied with a water-cooling system and gas-in/gas-out equipment for keeping a protective atmosphere) is put directly on the XY-motorized stage of the Horiba HR800 system. For in-situ measurements, laser can be focused on the sample at desired regions through a quartz window. Controlled heating/holding/cooling can be realized at a temperature range from room temperature to 1000 °C during the in-situ experiments.

Supporting Information

Supporting Information is available from the Wiley Online Library or from the author.

Acknowledgements

This work was supported by MOST (2011YQ0301240201 and 2011CB932601) and NSFC (21233001, 50972001, 51121091 and 21129001).

Received: October 18, 2012
Revised: November 29, 2012
Published online: January 6, 2013

[1] M. Fleischmann, P. J. Hendra, A. J. McQuillan, *Chem. Phys. Lett.* **1974**, *26*, 163–166.
[2] M. G. Albrecht, J. A. Creighton, *J. Am. Chem. Soc.* **1977**, *99*, 5215–5217.
[3] D. L. Jeanmaire, R. P. Van Duyne, *J. Electroanal. Chem.* **1977**, *84*, 1–20.
[4] K. Kneipp, Y. Wang, H. Kneipp, L. T. Perelman, I. Itzkan, R. Dasari, M. S. Feld, *Phys. Rev. Lett.* **1997**, *78*, 1667–1670.
[5] S. M. Nie, S. R. Emory, *Science* **1997**, *275*, 1102–1106.
[6] E. C. Le Ru, P. G. Etchegoin, *Principles of Surface-Enhanced Raman Spectroscopy and related plasmonic effects*, Elsevier, Amesterdam, **2009**.
[7] X. M. Lin, Y. Cui, Y. H. Xu, B. Ren, Z. Q. Tian, *Anal. Bioanal. Chem.* **2009**, *394*, 1729–1745.
[8] J. F. Li, Y. F. Huang, Y. Ding, Z. L. Yang, S. B. Li, X. S. Zhou, F. R. Fan, W. Zhang, Z. Y. Zhou, D. Y. Wu, B. Ren, Z. L. Wang, Z. Q. Tian, *Nature* **2010**, *464*, 392–395.
[9] W. G. Xu, X. Ling, J. Q. Xiao, M. S. Dresselhaus, J. Kong, H. X. Xu, Z. F. Liu, J. Zhang, *Proc. Natl. Acad. Sci. USA* **2012**, *109*, 9281–9286.
[10] X. Y. Zhang, J. Zhao, A. V. Whitney, J. W. Elam, R. P. Van Duyne, *J. Am. Chem. Soc.* **2006**, *128*, 10304–10309.
[11] X. Gong, Y. Bao, C. Qiu, C. Jiang, *Chem. Commun.* **2012**, *48*, 7003–7018.
[12] H. Cang, A. Labno, C. Lu, X. Yin, M. Liu, C. Gladden, Y. Liu, X. Zhang, *Nature* **2011**, *469*, 385–388.
[13] D. D. Dlott, Y. Fang, N. H. Seong, *Science* **2008**, *321*, 388–392.
[14] K. S. Novoselov, A. K. Geim, S. V. Morozov, D. Jiang, Y. Zhang, S. V. Dubonos, I. V. Grigorieva, A. A. Firsov, *Science* **2004**, *306*, 666–669.
[15] A. K. Geim, K. S. Novoselov, *Nat. Mater.* **2007**, *6*, 183–191.
[16] M. Freebody, *Photonic. Spectra* **2010**, *44*, 25–26.
[17] L. M. Malard, M. A. Pimenta, G. Dresselhaus, M. S. Dresselhaus, *Phys. Rep.* **2009**, *473*, 51–87.
[18] P. H. Tan, W. P. Han, W. J. Zhao, Z. H. Wu, K. Chang, H. Wang, Y. F. Wang, N. Bonini, N. Marzari, N. Pugno, G. Savini, A. Lombardo, A. C. Ferrari, *Nat. Mater.* **2012**, *11*, 294–300.
[19] N. Jung, N. Kim, S. Jockusch, N. J. Turro, P. Kim, L. Brus, *Nano Lett.* **2009**, *9*, 4133–4137.
[20] H. T. Liu, S. M. Ryu, Z. Y. Chen, M. L. Steigerwald, C. Nuckolls, L. E. Brus, *J. Am. Chem. Soc.* **2009**, *131*, 17099–17101.
[21] L. M. Xie, X. Ling, Y. Fang, J. Zhang, Z. F. Liu, *J. Am. Chem. Soc.* **2009**, *131*, 9890–9891.
[22] X. Ling, L. Xie, Y. Fang, H. Xu, H. Zhang, J. Kong, M. S. Dresselhaus, J. Zhang, Z. Liu, *Nano Lett.* **2010**, *10*, 553–561.
[23] S. Huh, J. Park, Y. S. Kim, K. S. Kim, B. H. Hong, J. M. Nam, *ACS Nano* **2011**, *5*, 9799–9806.
[24] X. Ling, J. Zhang, *Small* **2010**, *6*, 2020–2025.
[25] X. Ling, J. X. Wu, W. G. Xu, J. Zhang, *Small* **2012**, *8*, 1365–1372.

[26] H. Xu, L. M. Xie, H. L. Zhang, J. Zhang, *ACS Nano* **2011**, *5*, 5338–5344.
[27] H. Xu, Y. B. Chen, W. G. Xu, H. L. Zhang, J. Kong, M. S. Dresselhaus, J. Zhang, *Small* **2011**, *7*, 2945–2952.
[28] Y. Y. Wang, Z. H. Ni, H. L. Hu, Y. F. Hao, C. P. Wong, T. Yu, J. T. L. Thong, Z. X. Shen, *Appl. Phys. Lett.* **2010**, *97*, 163111.
[29] G. Lu, H. Li, C. Liusman, Z. Y. Yin, S. X. Wu, H. Zhang, *Chem. Sci.* **2011**, *2*, 1817–1821.
[30] X. J. Liu, L. Y. Cao, W. Song, K. L. Ai, L. H. Lu, *ACS Appl. Mater. Interfaces* **2011**, *3*, 2944–2952.
[31] W. Ren, Y. X. Fang, E. K. Wang, *ACS Nano* **2011**, *5*, 6425–6433.
[32] E. C. Le Ru, P. G. Etchegoin, M. Meyer, *J. Chem. Phys.* **2006**, *125*, 204701-1–204701-13.
[33] D. S. L. Abergel, A. Russell, V. I. Fal'ko, *Appl. Phys. Lett.* **2007**, *91*, 063125-1–063125-3.
[34] S. Roddaro, P. Pingue, V. Piazza, V. Pellegrini, F. Beltram, *Nano Lett.* **2007**, *7*, 2707–2710.
[35] H. Q. Zhou, C. Y. Qiu, Z. Liu, H. C. Yang, L. J. Hu, J. Liu, H. F. Yang, C. Z. Gu, L. F. Sun, *J. Am. Chem. Soc.* **2010**, *132*, 944–946.
[36] Z. T. Luo, L. A. Somers, Y. P. Dan, T. Ly, N. J. Kybert, E. J. Mele, A. T. C. Johnson, *Nano Lett.* **2010**, *10*, 777–781.
[37] C. Y. Liu, K. C. Liang, W. L. Chen, C. H. Tu, C. P. Liu, Y. Tzeng, *Opt. Express* **2011**, *19*, 17092–17098.
[38] S. S. Chen, L. Brown, M. Levendorf, W. W. Cai, S. Y. Ju, J. Edgeworth, X. S. Li, C. W. Magnuson, A. Velamakanni, R. D. Piner, J. Y. Kang, J. Park, R. S. Ruoff, *ACS Nano* **2011**, *5*, 1321–1327.